Molecular Cell
Article

A Tethering Mechanism Controls the Processivity and Kinetochore-Microtubule Plus-End Enrichment of the Kinesin-8 Kif18A

Jason Stumpff,[2,4] Yaqing Du,[1,4] Chauca A. English,[1] Zoltan Maliga,[3] Michael Wagenbach,[2] Charles L. Asbury,[2] Linda Wordeman,[2,4,*] and Ryoma Ohi[1,4,*]
[1]Department of Cell and Developmental Biology, Vanderbilt University Medical Center, Nashville, TN, 37232
[2]Department of Physiology and Biophysics, University of Washington School of Medicine, Seattle, WA, 98195
[3]Max Planck Institute of Molecular Cell Biology and Genetics, Dresden, Germany
[4]These authors contributed equally to this work
*Correspondence: ryoma.ohi@vanderbilt.edu (R.O.), worde@u.washington.edu (L.W.)
DOI 10.1016/j.molcel.2011.07.022

SUMMARY

Metaphase chromosome positioning depends on Kif18A, a kinesin-8 that accumulates at and suppresses the dynamics of K-MT plus ends. By engineering Kif18A mutants that suppress MT dynamics but fail to concentrate at K-MT plus ends, we identify a mechanism that allows Kif18A to accumulate at K-MT plus ends to a level required to suppress chromosome movements. Enrichment of Kif18A at K-MT plus ends depends on its C-terminal tail domain, while the ability of Kif18A to suppress MT growth is conferred by the N-terminal motor domain. The Kif18A tail contains a second MT-binding domain that diffuses along the MT lattice, suggesting that it tethers the motor to the MT track. Consistently, the tail enhances Kif18A processivity and is crucial for it to accumulate at K-MT plus ends. The heightened processivity of Kif18A, conferred by its tail domain, thus promotes concentration of Kif18A at K-MT plus ends, where it suppresses their dynamics to control chromosome movements.

INTRODUCTION

During congression, mitotic chromosomes are maneuvered toward the spindle midpoint around which they establish a metastable pattern of oscillations (Skibbens et al., 1993). This dynamic state is referred to as metaphase chromosome alignment and requires continuous coupling between kinetochore movement and kinetochore-microtubule (K-MT) plus ends. Recent work has established that eukaryotic cells employ members of the kinesin-8 subfamily to achieve chromosome alignment. The human kinesin-8, Kif18A, promotes chromosome alignment by suppressing the oscillatory movements of mitotic chromosomes. In the absence of Kif18A, kinetochores exhibit increased oscillation amplitudes leading them away from the metaphase plate, whereas overexpression of Kif18A causes kinetochores to cease oscillating in favor of tight alignment at the plate (Jaqaman et al., 2010; Stumpff et al., 2008). Since Kif18A suppresses MT growth in vitro (Du et al., 2010), it is likely that Kif18A dampens chromosome movements through direct suppression of K-MT plus-end dynamics. The ability of kinesin-8s to form a length-dependent gradient along MTs (Mayr et al., 2007; Stumpff et al., 2008; Tischer et al., 2009; Varga et al., 2006) suggests that this family of motors may modify K-MT plus-end dynamics in a length-dependent manner. Therefore, determining the mechanism(s) by which Kif18A accumulates in a graded manner at K-MT plus ends is an important step toward understanding how mitotic chromosome movements and alignment are controlled.

In animal cells, the enrichment of Kif18A at the plus ends of metaphase K-MTs, which average ~6 μm in length, depends on its plus-end-directed motility (Stumpff et al., 2008). Assuming that Kif18A lands at random locations along K-MTs, the motor is faced with the challenge of having to traverse a distance that is unusually long for kinesin-like proteins (Vale et al., 1996). This is particularly true for long K-MTs that are attached to kinetochores positioned beyond the spindle equator, the plus ends of which are thought to be the primary site of action of Kif18A motors (Stumpff et al., 2008). A key question is whether Kif18A undergoes prolonged periods of motility, a behavior termed "processivity," in order to efficiently target K-MT plus ends regardless of their length (Varga et al., 2006; Varga et al., 2009). Increased dwell times at K-MT plus ends, due either to slow dissociation of the motor or to recognition of structural features that are specific to plus ends (Peters et al., 2010), might also contribute to gradient formation. In order to determine if Kif18A is capable of meeting these biophysical demands, it is essential to measure the motility parameters of single Kif18A motors in isolation.

Here, we utilized a single-molecule total internal reflection fluorescence (TIRF) microscopy assay to demonstrate that Kif18A is a highly processive motor and that this processivity is significantly enhanced by a nonmotor MT-binding activity located within the tail domain of Kif18A. Mutants lacking the tail domain retain the ability to suppress MT plus-end dynamics in vitro, but fail to show a graded distribution along K-MTs and are incapable of suppressing chromosome movements in cells.

In accord with our single-molecule data, we find that a tailless Kif18A mutant interacts only transiently with the mitotic spindle, suggesting that reduced processivity explains the inability of the mutant to localize to K-MT plus ends. Enhanced processivity provided by the Kif18A tail is thus a requirement to accumulate Kif18A motor at K-MT plus ends to a concentration sufficient for suppression of MT dynamics. Using this mechanism, Kif18A controls chromosome movements by suppressing K-MT plus-end dynamics in a concentration- and motor-domain-dependent manner.

RESULTS

Kif18A Turnover at K-MT Plus Ends Depends on MT Dynamics

We used fluorescence recovery after photobleaching (FRAP) to characterize the behavior of K-MT plus-end-localized Kif18A-GFP. Because Kif18A overexpression is detrimental to mitosis (Du et al., 2010; Stumpff et al., 2008), we used a HeLa cell line created by BAC recombineering (Poser et al., 2008) that stably expresses a single additional copy of Kif18A with GFP fused to its C terminus. The subcellular distributions of Kif18A-GFP in these cells closely matched previous descriptions (data not shown); in metaphase cells with well-aligned chromosomes, Kif18A-GFP localized along K-fibers and was concentrated at K-MT plus ends (Figure 1A). Notably, kinetochores oscillated with decreased amplitudes in the Kif18A-GFP cell line (Figure S1), indicating that a modest 2-fold increase in Kif18A protein levels affects kinetochore movements. When K-MT plus-end-bound Kif18A-GFP was regionally photobleached with a UV laser, we observed a partial recovery of fluorescence, indicating replacement of bleached Kif18A-GFP molecules with unbleached motor. Fluorescence recovery at K-MT plus ends was rapid and fit well with single exponential kinetics, with a half-life of recovery ($t_{1/2}$) equal to ~9.5 ± 1.2 s (mean ± SEM) (Figure 1B and Table S1). A conspicuous characteristic of Kif18A-GFP recovery at K-MT plus ends is that it was invariably partial; on average, we measured that 29.5 ± 3.1% of Kif18A-GFP fluorescence did not recover (n = 17 kinetochores) (Figure 1B). These data suggest that, in the Kif18A-GFP transgenic cell line, a significant fraction of Kif18A-GFP molecules is stably associated with K-MT plus ends.

We surmised that the two populations of Kif18A at K-MT plus ends could reflect heterogeneity in the dynamics of K-MT plus ends: fast turnover might take place on dynamic K-MT plus ends that undergo repeated cycles of tubulin subunit loss and addition, whereas slow turnover might occur on stable K-MT plus ends. To test this, we used time-lapse microscopy to image Kif18A-GFP behavior in cells exposed to 10 μM taxol, a treatment that stabilizes MT plus ends. Taxol administration to metaphase cells caused a time-dependent redistribution of Kif18A-GFP from spindle MTs and K-MT plus ends to equatorially localized puncta (Figure 1C and Movie S1), which we confirmed to be K-MT plus ends by costaining with anti-kinetochore antibodies (CREST serum) in fixed cells (Figure 1D). At early time points (60 s), Kif18A-GFP also appeared at astral MT plus ends (Figure S2A), suggesting that Kif18A does not discriminate between K-MT and non-K-MT plus ends, but rather becomes enriched on the plus ends of stable MTs. Accumulation of Kif18A-GFP at K-MT plus ends was evident at 5 min following drug addition and reached maximal levels within ~10 min. By FRAP, we found that Kif18A-GFP exhibited dramatically reduced turnover at K-MT plus ends in taxol-treated cells (Figures 1E and 1F); an average of 9.2 ± 3.1% fluorescence at K-MT plus ends recovered following photobleaching (n = 11 kinetochores). This observation strongly suggests that Kif18A turnover at K-MT plus ends is coupled to MT dynamics.

The Tail Domain of Kif18A Is Essential for the Motor to Concentrate at K-MT Plus Ends

Although the localization of Kif18A to K-MT plus ends requires motility (Stumpff et al., 2008), how the motor is able to walk the length of a half-spindle is unclear. To determine the regions of Kif18A that are required for localization to K-MT plus ends, we created a series of GFP-tagged Kif18A truncation mutants and analyzed the distributions of these proteins in mitotic HeLa cells. Like full-length Kif18A (Kif18A-FL), two minimal dimeric motors (amino acids 1-406 and 1-480; GFP-Kif18A-N406 and Kif18A-N480-GFP) were able to bind spindle MTs, consistent with the motor domain possessing MT-binding activity. However, the C-terminally truncated motors did not accumulate at K-MT plus ends, suggesting a key role for the tail in MT plus-end targeting. Interestingly, GFP fused to the tail alone (aa 591-898; GFP-Kif18A-C307) exhibited spindle localization, but did not localize to kinetochores as reported for *Drosophila melanogaster* Klp67A (Savoian and Glover, 2010). Thus, K-MT plus-end targeting of human Kif18A requires its motile motor domain and its C-terminal tail domain (Figures 2A and 2B), *neither* of which are capable of targeting without the other.

To gain further insight into how the tail promotes the K-MT plus-end enrichment of Kif18A, we examined the redistribution of Kif18A-N480-GFP following taxol treatment (Figure S2B). In contrast to full-length Kif18A, Kif18A-N480-GFP accumulated only modestly at K-MT plus ends in taxol-treated cells. The tailless motor also decorated the lattice of both spindle and astral MTs, a result we confirmed by live imaging (Movie S2). The Kif18A tail thus promotes robust MT plus-end localization of the motor in a manner that is independent of MT plus-end stability. We reasoned that reduced MT binding of tailless Kif18A motors could underlie the inability of these truncation mutants to target K-MT plus ends. If this were the case, the residence time of tailless Kif18A on spindle MTs should be reduced relative to full-length Kif18A. To investigate this possibility, we used photoconversion to regionally mark either full-length tdEOS-Kif18A or Kif18A-N480-tdEOS fusions on half-spindles in HeLa cells and quantified fluorescence intensities within the photomarked regions over time (Figure 2C). Residence times of the two motors on spindle MTs were fit with single exponential kinetics (Figure 2D), with full-length Kif18A exhibiting a half-life of 69 s (n = 8). Fluorescence of Kif18A-N480-tdEOS dissipated quickly with a half-life of 15.9 s following photoconversion (n = 11) (Figures 2C and 2D). Collectively, these results suggest that the tail domain of Kif18A is essential for the motor to concentrate at K-MT plus ends and that it acts by increasing the residence time of Kif18A on spindle MTs.

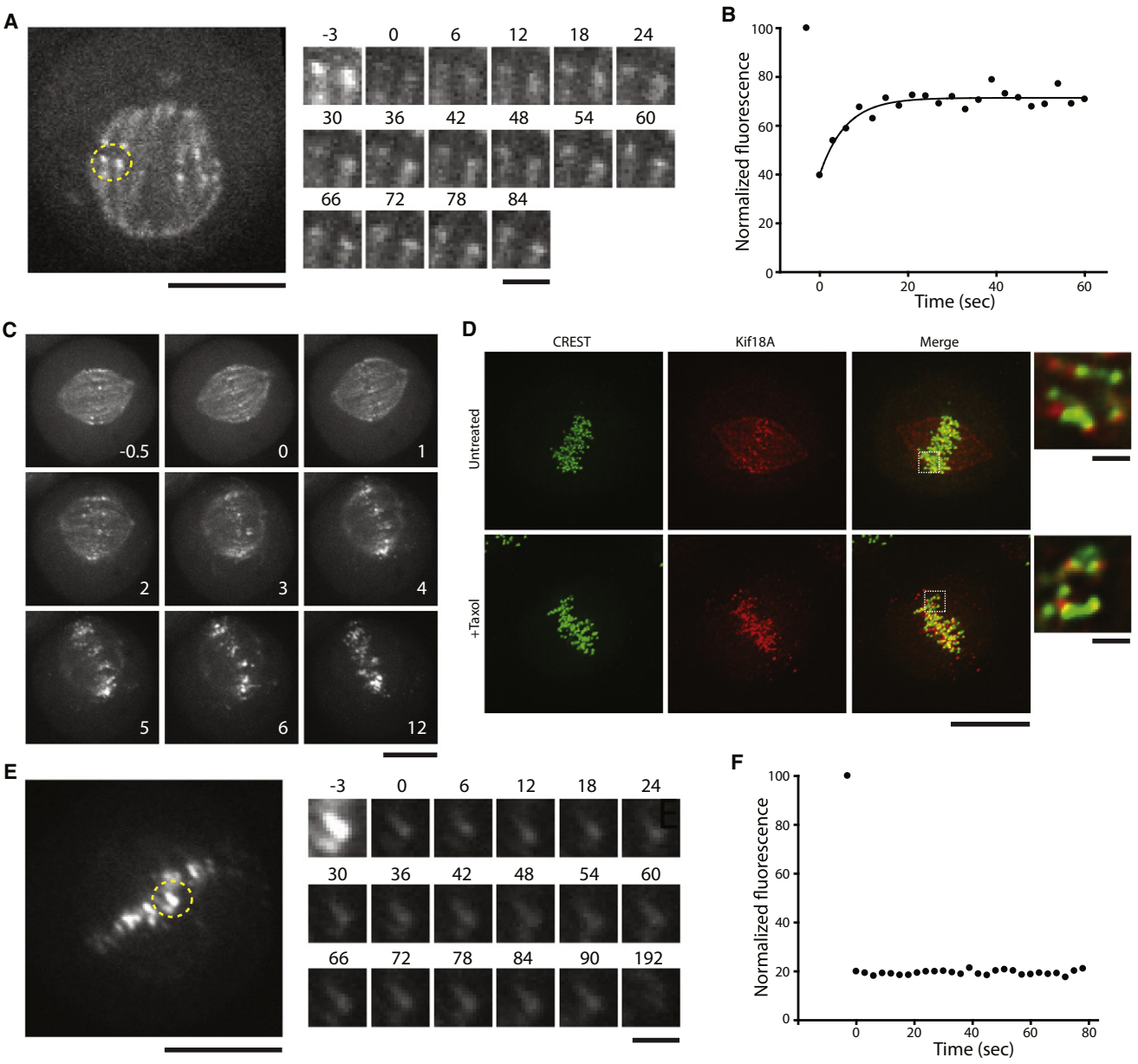

Figure 1. MT Dynamics Govern Kif18A Turnover at K-MT Plus Ends

(A) Photobleaching of Kif18A-GFP in a metaphase HeLa cell. Irradiation was targeted to the indicated region (dashed yellow line). Enlarged images show K-MT plus-end fluorescence before and after photobleaching. Time is indicated in s and is relative to irradiation. Scale bars, 10 μm and 2 μm (enlarged images).

(B) Kinetics of Kif18A-GFP fluorescence recovery at a K-MT plus end. A representative plot of normalized Kif18A-GFP fluorescence at a single kinetochore against time is shown. The recovery of Kif18A-GFP at K-MT plus ends fit a single exponential (black line).

(C) Taxol causes equatorial enrichment of Kif18A-GFP. Still images from a video of a HeLa cell stably expressing Kif18A-GFP treated with 10 μM taxol. Time is indicated in min and is relative to taxol addition. Scale bar, 10 μm.

(D) Kif18A is enriched at kinetochores in taxol-treated HeLa cells. The localizations of endogenous Kif18A (red) and kinetochores (green) in a control HeLa cell or in a cell treated with 10 μM taxol for 15 min are shown. Insets are higher magnification views of the boxed regions. Scale bars, 10 μm and 1 μm (enlarged images).

(E) Photobleaching of Kif18A-GFP in a taxol-treated metaphase HeLa cell. Time is indicated in s and is relative to irradiation. Scale bars, 10 μm and 2 μm (enlarged images).

(F) Kinetics of Kif18A-GFP fluorescence recovery at a K-MT plus end in a cell treated with 10 μM taxol. A representative plot of normalized Kif18A-GFP fluorescence at a single kinetochore against time is shown.

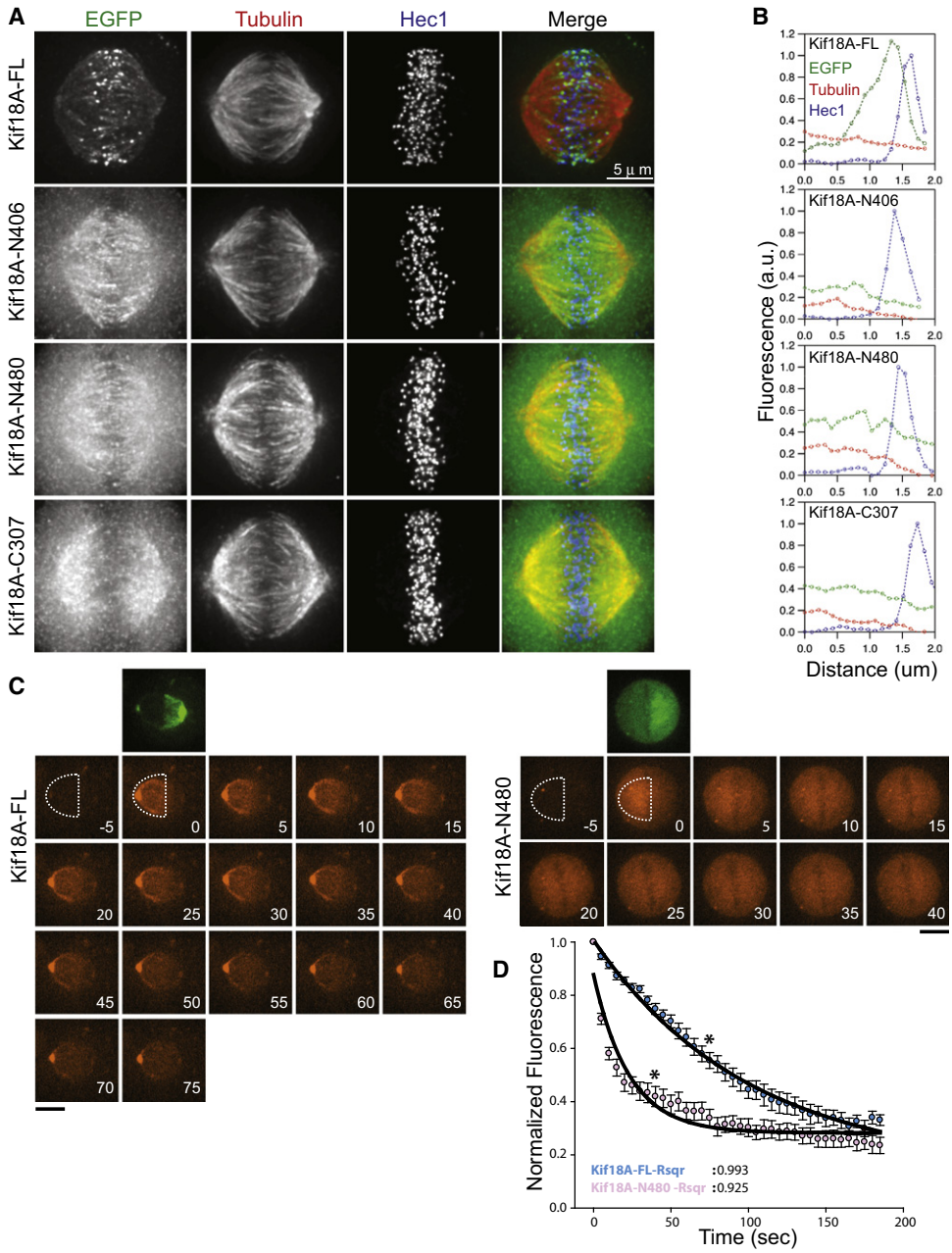

Figure 2. The C-Terminal Tail Domain of Kif18A Is Required for the Motor to Target K-MT Plus Ends

(A) Metaphase localization of Kif18A truncation mutants. The localizations of full-length GFP-Kif18A, GFP-Kif18A-N406, Kif18A-N480-GFP, and GFP-Kif18A-C307 in cells costained for tubulin (red) and Hec1 (blue) are shown. Scale bar, 5 μm.

(B) The C-terminal tail domain of Kif18A is required for the motor to accumulate at K-MT plus ends. Representative linescans showing the distribution of Kif18A (green) along metaphase K-MTs (red) near the kinetochore (Hec1 peak, blue).

(C) The tail domain of Kif18A increases the dwell time of the motor on spindle MTs. Still images from photoconversion runs of tdEOS-Kif18A-FL and Kif18A-N480-tdEOS are shown. An image of fluorescence from the GFP channel is shown at the moment of photoconversion (t = 0). Regions that were photoconverted and subjected to analysis are outlined. Time is indicated in s and is relative to the time of photoconversion. Scale bar, 10 μm.

(D) Decay kinetics of tdEOS-Kif18A-FL (blue) and Kif18A-N480-tdEOS (pink) fluorescence from the mitotic spindle. Normalized mean fluorescence of photoconverted tdEOS-Kif18A-FL (n = 8) and Kif18A-N480-tdEOS (n = 11) versus time in s are shown. Asterisks denote time points corresponding to the final images shown in Figure 2C. Black lines represent fits of the data to single exponentials. Error bars represent SEM.

The C Terminus of Kif18A Enhances Processivity but Decreases Velocity

To characterize the motile properties of Kif18A-FL and tailless Kif18A, we first used conventional MT gliding assays with varying concentrations of purified coverslip-bound motor (Figures 3A and S3). Filament sliding powered by tailless Kif18A was faster than Kif18A-FL at all concentrations tested. At 500 nM, the highest motor concentration examined, MTs were translocated by Kif18A-FL at 128.2 ± 4.2 nm sec^{-1} (mean ± SEM, n = 31) (Figure 3A). Kif18A-FL-GFP behaved similarly in this assay, but 500 nM Kif18A-N480-GFP powered MT gliding at speeds 1.4-fold faster than Kif18A-GFP-FL (174.0 ± 2.2 nm sec^{-1} [n = 30] versus 126.3 ± 2.4 nm sec^{-1} [n = 34]) and untagged Kif18A-FL. Notably, like Kif18A-FL (Du et al., 2010), we observed that Kif18A-N480-GFP did not depolymerize GMPCPP MTs (Figure S4). These observations suggest that the tail domain of Kif18A slows the overall motility of the motor domain.

To further analyze the effects of Kif18A's tail domain on its motility, we measured the behavior of full-length and tailless Kif18A molecules on MTs using a single-molecule TIRF microscopy assay. Under conditions where Kif18A is tightly associated with MTs, the fluorescence of both GFP-labeled full-length and tailless Kif18A molecules was always reduced to background levels in one or two steps, indicating that we were indeed imaging single molecules of Kif18A (Figure 3B). The motility of full-length and tailless Kif18A was then analyzed in assay buffers with various ionic strengths. Under the lowest salt concentrations tested (BRB80 + 75 mM KCl), we observed that both GFP-Kif18A-FL and GFP-Kif18A-N406 moved processively along MTs for long distances that were often limited by the length of the MT (Figures 3C–3E and Movies S3–S4). However, the dissociation rate from the MT measured for GFP-Kif18A-N406 was increased relative to that of GFP-Kif18A-FL (Figures 3F and S5). The dissociation rate for GFP-Kif18A-N406 was further increased at higher ionic strengths, leading to shorter run-lengths along the MT on average (Figures 3D–3F and S5). In contrast, the dissociation rate and run-lengths of GFP-Kif18A-FL molecules were less sensitive to changes in ionic strength (Figures 3D–3F, S5, and Movie S4). We also observed that both GFP-Kif18A-FL and GFP-Kif18A-N406 could remain associated with MT tips for extended periods of time (Figures 3C and 3D), but that the tip dwell time of the tailless mutant was reduced 5.6-fold compared to that of the full-length protein under conditions where both motors displayed relatively high processivity (BRB80 + 100 mM KCl) (Figure 3G). Similar to our measurements from gliding filament assays, we also observed that the velocity of GFP-Kif18A-N406 was increased 2.5-fold compared to GFP-Kif18A-FL, but neither motor construct displayed significant salt-sensitive changes in velocity (Figures 3H and S5). These data indicate that the Kif18A tail functions to prevent the release of the motor from the MT, thus increasing its processivity.

The Tail Domain Harbors a Nonmotor MT-Binding Site

In interphase HeLa cells, transiently overexpressed GFP-Kif18A-C307, but not GFP, localized to what appeared to be bundles of MTs based on tubulin immunofluorescence (Figure 4A). This result, combined with the observation that the tail alone localizes to the mitotic spindle (Figure 2A), suggests that the tail domain may directly bind MTs via a second MT-binding site. To test this hypothesis, we incubated recombinant GFP-tagged Kif18A-C307 with rhodamine-labeled GMPCPP MTs. MTs were bundled in the presence of Kif18A-C307-GFP, and GFP fluorescence was evident along MT bundles (Figure 4B). We used an MT cosedimentation assay to verify the tail-MT interaction, incubating a fixed concentration of tail protein (250 nM) with varying amounts of taxol-stabilized MTs. Although negligible amounts of the tail pelleted in the absence of MTs, Kif18A-C307 copelleted with MTs in a concentration-dependent manner (Figure 4C). The tail binds MTs with an apparent affinity of 0.36 μM, which is likely an upper limit, given the similarity of this value to the concentration of tail protein used in our assay (Figure 4D). Since the run length of the tailless motor is sensitive to changes in ionic strength, we tested the effect of salt on the ability of the tail to copellet with MTs. The amount of tail that copelleted with MTs decreased by 14.6% and 41.9% in buffer containing 150 and 300 mM KCl, respectively (Figure 4D). In addition, the apparent affinity of tail-MT interactions were reduced with increasing ionic strength (K_d, 150 mM KCl = 0.58 μM, and K_d; 300 mM KCl = 1.29 μM). These results suggest that tail-MT interactions are at least in part electrostatic in nature.

The MT-binding activity of the Kif18A tail and its effect on the residence time of the motor suggest that it may act as a tether to prevent Kif18A from dissociating from the MT. To investigate the behavior of the Kif18A tail alone on MTs, we analyzed individual binding events between Kif18A-C307-GFP and taxol-stabilized MTs, using a single-molecule TIRF assay. The brightness of the Kif18A-C307-GFP particles (18,626 ± 8025 a.u.) was very similar to that of a GFP-tagged monomeric MCAK control imaged in parallel (15,815 ± 7623), indicating that these were Kif18A tail monomers tagged with a single GFP (Figures 5A–5C). Kif18A-C307-GFP exhibited short diffusive movements along the MT lattice with a dissociation rate of 1.16 ± 0.07 s^{-1} and an apparent diffusion coefficient of 0.019 ± 0.003 um^2s^{-1} (Figures 5D and 5E and Movie S5). This behavior is consistent with the idea that the tail associates with MTs via electrostatic interactions and suggests that it could act as a sliding tether to prevent Kif18A from dissociating from the MT.

Suppression of MT Dynamics by Kif18A Is Mediated Exclusively by Its Motor Domain

In addition to tethering Kif18A to the MT lattice, the tail domain could contribute to Kif18A's function in suppressing MT plus-end dynamics. To test this, we compared the abilities of Kif18A-FL- GFP and Kif18A-N480-GFP to block MT growth off of axonemal plus ends. In reactions of low ionic strength (BRB80 + 75 mM KCl) and high motor concentration (500 nM), both motors accumulated at axonemal plus ends, but Kif18A-N480-GFP also labeled the axoneme lattice (Figure 6A), consistent with the notion that the tail domain increases the ability of the motor to translocate to plus ends. We measured the lengths of MTs with GFP-positive ends and found that Kif18A-N480-GFP blocks MT assembly off of plus ends with potency similar to that of Kif18A-FL. In control reactions, long MTs grown off plus ends averaged 9.63 ± 0.42 μm (n = 161) in length, whereas

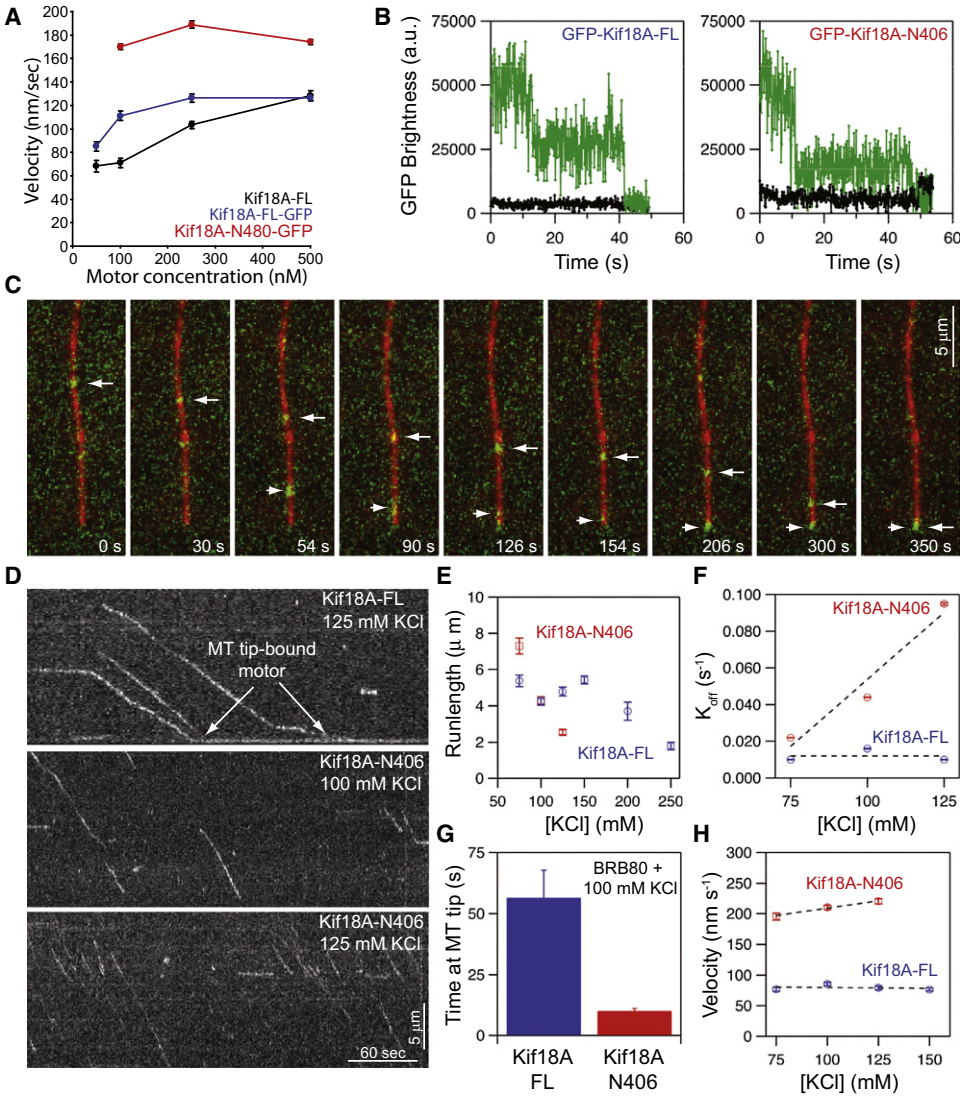

Figure 3. Kif18A's Tail Domain Increases Kif18A's Processivity and Reduces Both Its Velocity and Dissociation Rate from Microtubules

(A) Gliding filament velocities measured in assays with varying concentrations of the indicated Kif18A motors bound to the coverslip.

(B) Representative examples of GFP brightness (green trace) from measurements of GFP-Kif18A-FL and GFP-Kif18A-N406 under conditions where the motors are tightly bound to the microtubule. GFP-Kif18A particles always displayed one or two photobleach steps indicating that they are single molecules.

(C) Stills from a time-lapse showing the long processive movement and MT end-binding activity displayed by single molecules of GFP-Kif18A-FL (marked by white arrows). Elapsed time is reported in s.

(D) Representative kymographs showing the movement of single GFP-Kif18A-FL and GFP-Kif18A-N406 molecules along taxol MTs in BRB80 buffer plus the indicated concentration of KCl.

(E–G) Single molecule experiments reveal that tailless, but not full-length, Kif18A displays reduced run lengths along the microtubule, as well as increased dissociation rates from both the MT lattice and tip. Plot of average run-lengths measured from analyses of single GFP-Kif18A-FL (blue points) and GFP-Kif18A-406 (red points) molecules as a function of KCl concentration (E); error bars represent SEM n = 320 (FL, 75 mM KCl), 421 (FL, 100 mM KCl), 396 (FL, 125 mM KCl), 455 (FL, 150 mM KCl), 62 (FL, 200 mM KCl), 63 (FL, 250 mM KCl) 205 (N406, 75 mM KCl), 458 (N406, 100 mM KCl), and 298 (N406, 125 mM KCl). Plot of average dissociation rate as a function of KCl concentration measured for the indicated motor constructs in single-molecule experiments (F); dissociation rates represent the inverse of the time constant from exponential fits to dwell-time distributions and are reported ± SD (see Figure S4). Plot of the average dwell time at the tip measured for the indicated motor construct in BRB80 + 100 mM KCl (G); error bars represent SEM n = 64 for Kif18A-FL and 40 for Kif18A-N406.

(H) Plot of average velocity as a function of KCl concentration measured from analyses of single GFP-Kif18A-FL and GFP-Kif18A-406 molecules. Error bars represent SEM, data set is the same as in (E). Data for all conditions are derived from at least three independent experiments.

MTs that polymerized off plus ends in the presence of Kif18A-FL-GFP or Kif18A-N480-GFP were 2.17 ± 0.14 μm (n = 153) and 1.54 ± 0.08 μm (n = 158), respectively (Figure 6B). This result indicates that the ability of Kif18A to suppress MT plus-end dynamics is contained within the motor domain itself and does not require the tail.

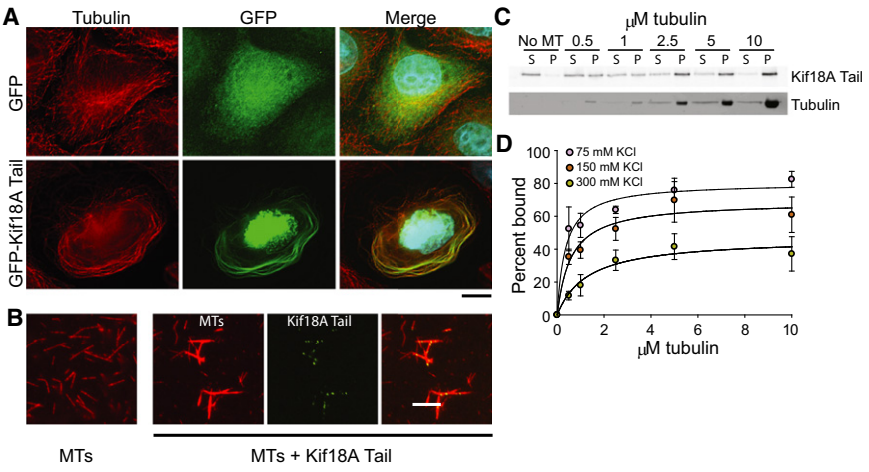

Figure 4. The Tail of Kif18A Contains a Second MT-Binding Site

(A) Overexpressed GFP-Kif18A-C307, but not GFP, localizes to and bundles interphase MTs. Representative tubulin-labeled (red) HeLa cells transfected with a GFP or GFP-Kif18A-C307 plasmid are shown. DNA was counterstained with Hoechst 33342. Scale bar, 10 μm.

(B) Kif18A-C307-GFP bundles MTs in vitro. Rhodamine-labeled GMPCPP MTs (red) were incubated with or without Kif18A-C307-GFP protein, as indicated. Panels show microscope fields after a 30 min incubation at room temperature. Scale bar, 10 μm.

(C) Kif18A-C307 binds MTs directly. An immunoblot of supernatant (S) and pellet (P) fractions from a MT cosedimentation assay of Kif18A-C307 in buffer containing 75 mM KCl with the indicated μM concentrations of polymerized tubulin is shown.

(D) Quantitative analysis of Kif18A-C307-MT binding in buffers of varying ionic strength. Data are averaged values from three independent experiments, where error bars indicate SEM.

To further investigate our hypothesis that the Kif18A tail promotes targeting of the motor to the ends of dynamic MTs but is not absolutely necessary for its ability to suppress MT dynamics, we evaluated the behavior of Kif18A-FL-GFP and Kif18A-N480-GFP on dynamic MTs in real time and under near-physiological conditions, using TIRF microscopy. In this assay, unlabeled dynamic MT seeds attached to the coverslip surface were used to nucleate Alexa 568-labeled MTs (Figure 6C). MTs grown in the absence of Kif18A were highly dynamic, undergoing alternating phases of assembly and disassembly (Figure 6E). Infusion of ATP and 25 nM Kif18A-FL-GFP led to the accumulation of motor at MT plus ends and the attenuation of MT growth. Strikingly, plus ends decorated with Kif18A-FL-GFP exhibited prolonged pausing, periods during which neither disassembly nor assembly were observed (Figures 6D and 6F). In contrast, the tailless motor failed to accumulate efficiently at MT plus ends, even at an 8-fold higher concentration (200 nM), and MTs remained dynamic under these conditions (Figure 6E). However, high concentrations of Kif18A-N480-GFP (1.6 μM) were able to induce pausing of MT plus ends. From these data, we conclude that Kif18A is a suppressor of MT plus-end dynamics and that this activity is conferred via its N-terminal domain. Furthermore, the tail is essential for the motor to efficiently accumulate at MT plus ends to a level that is sufficient to block MT plus-end dynamics.

Suppression of Chromosome Movements by Kif18A Requires It to Be a Processive Motor

Given that the Kif18A motor domain alone is sufficient to block MT plus-end assembly in vitro, we wanted to understand in greater detail the importance of the tail domain in K-MT plus-end regulation in cells. To examine this, we took advantage of

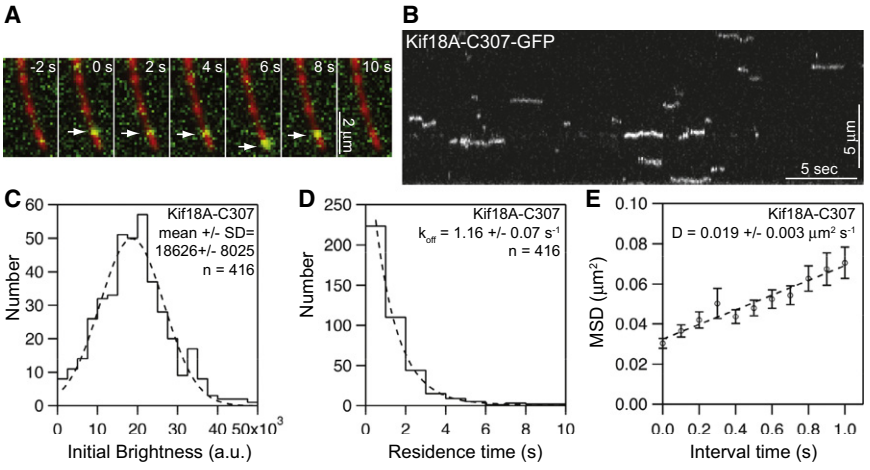

Figure 5. The Tail of Kif18A Diffuses along the MT Lattice

(A) Frames from a time-lapse showing diffusion of a single Kif18A-C307-GFP molecule near the tip of a taxol-stabilized MT.

(B) Kymograph displaying diffusive movements of Kif18A-C307-GFP molecules along an MT.

(C) Plot showing the distribution of initial brightness measurements made from analyses of Kif18A-C307-GFP molecules. A Gaussian fit (dotted line) to the distribution is shown and the mean ± SD is reported. n = number of spots analyzed.

(D) Plot of residence-time distribution for Kif18A-C307-GFP molecules. The dissociation rate derived from the exponential fit to the distribution (dotted line) is reported. n = 416.

(E) Plot of mean-squared displacement (MSD) at 0.1 s time intervals for Kif18A-C307-GFP. The dotted line shows the linear fit used to calculate the diffusion coefficient. n = 416.

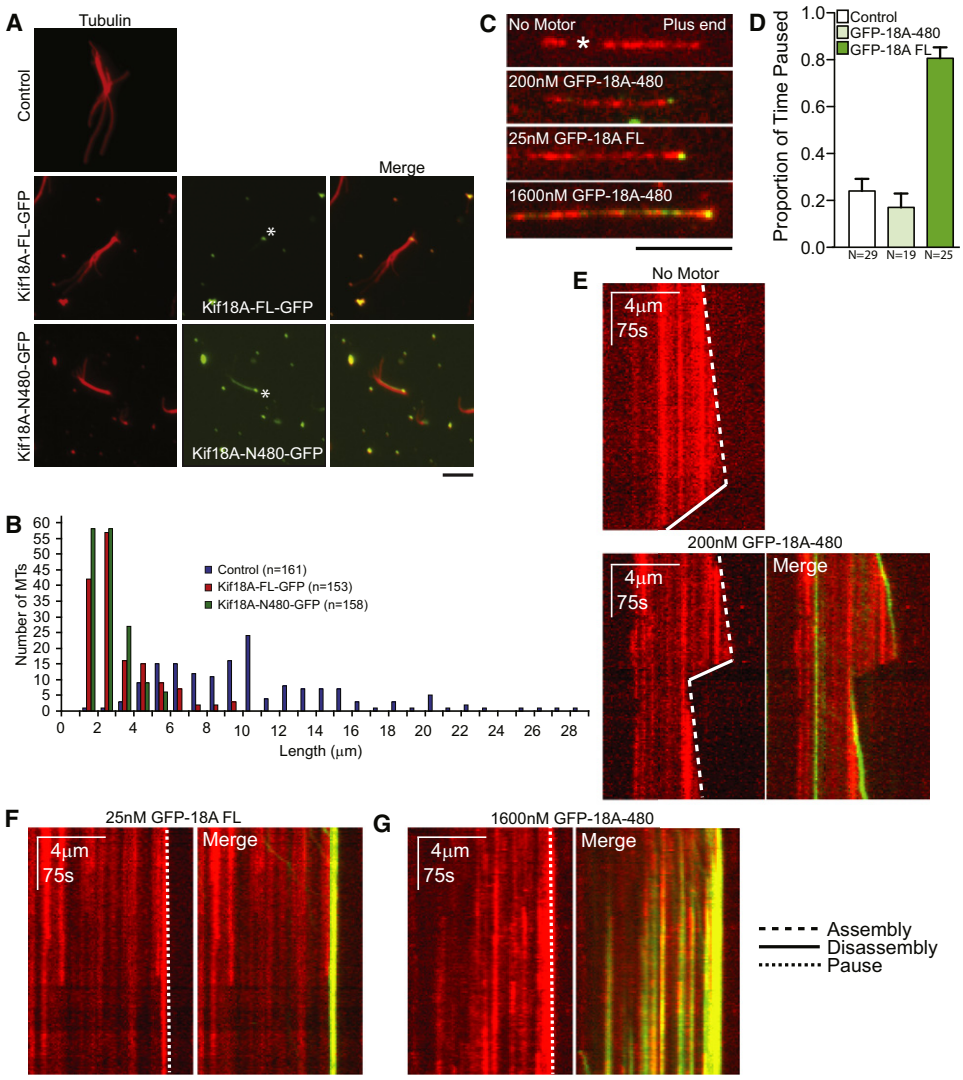

Figure 6. Suppression of MT Dynamics by Kif18A Is Mediated Exclusively by Its Motor Domain

(A) A tailless mutant of Kif18A blocks GTP-tubulin assembly off of axonemes. Axonemes were incubated with 20 μM tubulin at 37°C in the presence of buffer, 500 nM Kif18A-FL-GFP or 500 nM Kif18A-N480-GFP, and were fixed, sedimented onto coverslips, and stained for tubulin (red). Asterisks denote asymmetric enrichment of GFP-Kif18A proteins (green) on one axoneme end. Scale bar, 10 μm.

(B) Quantitation of axonemal MT lengths from (A). Histograms depict length distributions of MTs grown off of GFP-positive axoneme ends. n, number of MTs measured.

(C) Kif18A accumulates on the plus end of dynamic MTs in ATP. Unlabeled dynamic MT seed is indicated where visible (*). Scale bar, 4 μm.

(D) Twenty-five nanomolar full-length Kif18A-GFP (bright green) significantly increases the proportion of time spent in the pause state relative to no motor control (white) or 200 nM Kif18A-N480-GFP (light green). $p < 0.0001$.

(E) Two hundred nanomolar Kif18A-N480-GFP does not suppress MT dynamics. Kymographs show MT plus end behavior over time. A control MT (top) or an MT in the presence of 200 nM Kif18A-N480-GFP (bottom) exhibit normal dynamics.

(F) Twenty-five nanomolar full-length Kif18A-GFP leads to paused MTs.

(G) Kif18A-N480-GFP can induce MT pausing at high (1600 nM) concentrations.

the finding that overexpression of Kif18A-FL in metaphase cells causes a reduction in the amplitude of kinetochore oscillations (Stumpff et al., 2008). To determine the effect of the tail on Kif18A's ability to suppress chromosome movements, we tracked the movements of centromeres in HeLa cells expressing mRFP-CENP-B and quantified oscillation amplitudes using a previously developed metric, the deviation of kinetochores from an average position (DAP) (Stumpff et al., 2008). In control cells transfected with mRFP-CENP-B alone, sister centromeres exhibited a DAP of 0.21 ± 0.06 μm (Figures 7A–7C). As expected, cells overexpressing Kif18A-FL displayed an enrichment of the motor at kinetochores and a 34% decrease in DAP (0.14 ± 0.04 μm) (Figures 7A–7C). Kinetochores in cells transfected with Kif18A-N480-GFP, in contrast, behaved similarly to control

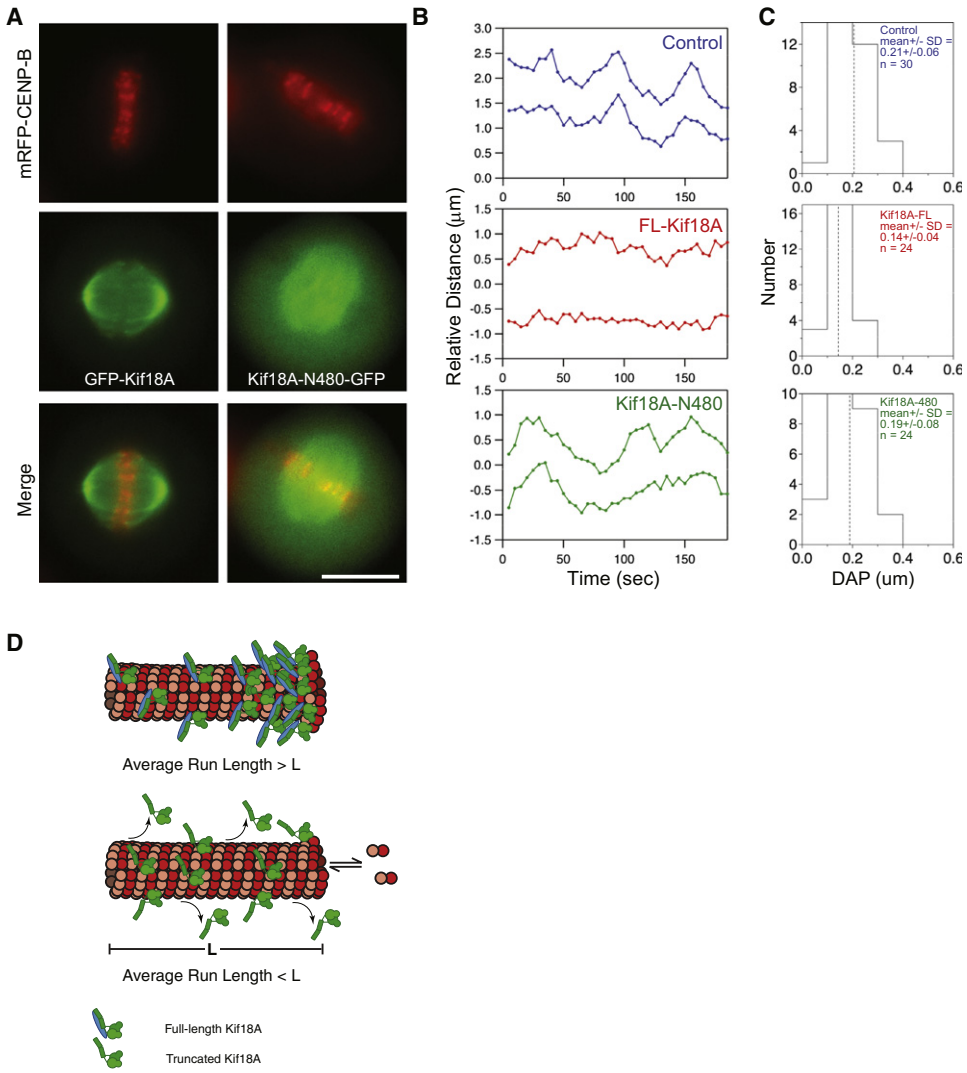

Figure 7. A Tailless Variant of Kif18A Is Unable to Dampen Kinetochore Oscillation Amplitude

(A) Representative still frames of mRFP-CENP-B (red) and full-length GFP-Kif18A or Kif18A-N480-GFP (green) in HeLa cells used to derive data in (B) and (C). Scale bar, 10 μm.

(B) Distance versus time plots of single kinetochore pairs from the indicated cell types. For all cells, images were collected every 5 s.

(C) Histograms showing deviation from average position (DAP) calculations for the indicated cell types. The mean ± SD is shown for each data set, and the mean value is marked by a vertical stippled line. n, number of kinetochores analyzed. The DAP for kinetochores in GFP-Kif18A-overexpressing cells are significantly different from the DAP for kinetochores in control cells ($p = 3.12 \times 10^{-5}$, two-sample t test). Kif18A-N480-GFP did not significantly alter the DAP for kinetochores relative to control cells ($p = 0.19$).

(D) Model. Two additional MT-binding sites located within the tail domains of a Kif18A homodimer allow this motor to be highly processive and traverse the length of a K-MT in the metaphase half-spindle of an animal cell (L). In the absence of the tail domain, the motor exhibits reduced run lengths and is unable to accumulate at MT plus ends in a graded fashion.

cells, despite a high level of motor overexpression (~3-fold higher than Kif18A-FL) (Figure S6). Kif18A-N480 did not concentrate appreciably at kinetochores or alter the localization of endogenous Kif18A (Figure S6B), and the mutant motor did not reduce chromosome oscillations (DAP = 0.19 ± 0.08 μm) (Figures 7A–7C). We conclude that, in cells, the tail domain is essential for Kif18A to target and therefore regulate the dynamics of K-MT plus ends.

DISCUSSION

A fundamental and conserved characteristic of the kinesin-8 motors is that they accumulate in a graded fashion along K-MTs, accumulating at MT plus ends (Stumpff et al., 2008; Tischer et al., 2009; Varga et al., 2006). The "antenna model" (Varga et al., 2009) postulates that kinesin-8 gradient profiles are MT length-dependent with longer MTs harboring higher

plus-end motor concentrations than shorter MTs. Based on this, it has been hypothesized that kinesin-8s can encode positional information through selectively altering the dynamics of long MTs (Stumpff et al., 2008; Tischer et al., 2009; Varga et al., 2006; Varga et al., 2009). This idea is consistent with the finding that the catastrophe frequency of klp5/6-decorated interphase MT bundles in fission yeast is positively correlated with bundle length (Tischer et al., 2009). Furthermore, preferential accumulation of kinesin-8s at K-MT plus ends that grow beyond the midzone could catalyze position-dependent directional switches in kinetochore movement, thereby constraining chromosome movements to the spindle equator (Stumpff et al., 2008). Evidence supporting the functional importance of the antenna model is lacking, however, partly because the biochemical mechanism(s) by which kinesin-8 proteins accumulate at MT plus ends is not known.

Our work demonstrates that the C-terminal tail domain of Kif18A is essential for the motor to accumulate at K-MT plus ends in a graded manner. Previously we established that a functional motor domain and, by extension, plus-end-directed motility was required to establish a gradient of Kif18A on K-MT plus ends in cells (Stumpff et al., 2008). However, our photoconversion studies reveal that, even in the presence of a functional motor domain, the association of tailless Kif18A with spindle MTs in cells is unstable, effectively preventing the motor from reaching K-MT plus ends. This result is consistent with our finding that the tail increases both the dwell time and processivity of individual Kif18A molecules on MTs at physiological salt concentrations in vitro. Our processivity measurements indicate that the full-length motor is capable of taking ~600 steps before dissociating from its MT track. This run length, which is an underestimate due to limitations imposed by the MT lengths in our assays, spans ~5 μm and is well within range to drive K-MT localization of Kif18A in the ~5–7 μm long metaphase half-spindle in animal cells. Consistent with our previous work (Du et al., 2010), we also found that single Kif18A molecules paused at the MT plus end, which agrees well with our observation that the full-length motor accumulates at and stably associates with K-MT plus ends in taxol-treated cells.

Our findings support a model (Figure 7D) in which MT-binding of the two tail domains of a Kif18A homodimer tether the motor domains to the MT track. We propose that the concerted activities of the four MT-binding sites underlie the unusually high processivity of Kif18A and other kinesin-8 motors. Indeed, the tail domain of Kip3 also promotes its accumulation at MT plus ends (Xiaolei Su and David Pellman, personal communication). Similarly, the tail domain of kinesin-5/Eg5, which also contains a nonmotor MT-binding site, performs an analogous function by allowing Eg5 to remain bound to one MT long enough for it to encounter a second MT of opposite polarity (Weinger et al., 2011). Also similar to kinesin-5, the tail of Kif18A slows the velocity of the motor ~2-fold. This self-repression was evident in single-molecule assays, where we observed slow movement and frequent pausing of individual full-length motors along the MT lattice. By contrast, tailless Kif18A motor constructs were derepressed and showed uninterrupted periods of motility. It is unlikely that the repressive effect imparted by the tail is due to tail-MT interactions because the predicted drag force of tail monomers based on our diffusion measurements (Bormuth et al., 2009) is small (~10 fN; data not shown) and therefore unlikely to significantly slow or stall the motor. We favor the hypothesis that, in addition to providing increased MT affinity, the tail may also function to reduce Kif18A movement by suppressing the ATPase activity of the motor domains, as is the case for conventional kinesin (Coy et al., 1999). It is also possible that the tail is capable of physically obstructing motor-track interactions. Testing these interesting hypotheses will be the subject of future experiments.

Our in vitro data suggest that the motor domain of Kif18A is largely responsible for its ability to suppress MT plus-end dynamics. This is consistent with the ability of the Kif18A motor domain alone to promote the formation of tubulin rings, i.e., deform tubulin protofilaments, in the presence of AMPPNP (Peters et al., 2010). Our TIRF experiments did reveal, however, that the tail is required for the motor to efficiently target MT plus ends to a level required for suppression of MT plus-end dynamics. Since the tail promotes both motor processivity and the ability of the motor to pause for extended lengths of time at the extreme MT plus end, the tail plays a key role in influencing flux of the motor through the plus end. It is thus likely that the reduced capacity of tailless Kif18A to suppress MT plus-end dynamics is due to its impaired ability to reach concentrations at the plus end that are required for activity. This concentration-dependent model to explain Kif18A action at the MT plus end is supported by our observation that tailless motor does associate and track with the ends of growing, and thus unaffected, MT plus ends in vitro.

Graded accumulation at MT plus ends is a unique characteristic of kinesin-8 motors, and it is likely that this property is central to the way that Kif18A controls chromosome movements. In sum, our data suggest a model in which Kif18A accumulates on K-MTs via tail-enhanced processivity and suppresses MT dynamics in a concentration-dependent manner. The model predicts that accumulation of a sufficient number of motors to suppress MT dynamics is positively correlated with the length of the K-fiber and dependent on the processivity of the motor. We speculate that such a mechanism would be especially important if a threshold of Kif18A activity at K-MT plus ends is required to significantly impact K-MT plus-end dynamics. In this case, a threshold concentration of Kif18A would suppress chromosome movement and prevent polymerization of long K-fibers that cross the spindle equator. Ultimately, this would tend to maneuver chromosomes to the spindle midzone and, once there, to preferentially restrict chromosome movements away from the spindle midpoint. Thus, the C-terminal tail of Kif18A is a vital regulatory module that promotes and enforces the equatorial positioning of chromosomes in mitotic cells.

EXPERIMENTAL PROCEDURES

Cell Culture and Transfections

HeLa "Kyoto" cells were cultured in DMEM containing 10% FCS plus antibiotics. HeLa Kyoto cells BAC-recombineered to express a single copy of Kif18A-GFP were cultured in DMEM containing 10% FCS, antibiotics, and 500 μg/ml G418. For live cell imaging, cells were plated onto 35 mm^2 glass coverslip dishes coated with poly-lysine (MatTek) ~24 hr prior to imaging

(Kif18A-GFP cells) or transfection. Plasmid DNA transfections were performed using either Lipofectamine 2000 (Invitrogen) or a Nucleofector electroporation system (Lonza) according to the manufacturer's instructions. Taxol was used at a final concentration of 10 μM.

Live Cell Imaging

To record kinetochore oscillations, HeLa cells transfected with mRFP-CENP-B and GFP fusions to either Kif18A-N480 or Kif18A-FL were imaged at 37°C in CO_2-independent media (Life Technologies), using a DeltaVision Core system (Applied Precision) equipped with an environmental chamber (Applied Precision). Methods to track and analyze kinetochore movements were described previously (Stumpff et al., 2008). For Kif18A-transfected cells, a single image was acquired in the GFP channel for each movie to gauge the level of protein overexpression. Five image planes spaced 0.5 μm apart were then acquired at 5 s intervals in the RFP channel, using a 60× 1.4 NA lens (Olympus) and a CCD camera.

Photobleaching, photoswitching, and taxol treatment experiments were performed on a Quorum WaveFX (Quorum Technologies) spinning disk confocal system controlled by MetaMorph imaging software (Universal Imaging Corp.), equipped with a Chamlide incubator set to 37°C (Live Cell Instrument).

Images were acquired using a 60× 1.49 NA objective (Nikon) and a back-thinned EM-CCD camera (Hamamatsu). For regional photomarking, a Mosaic Digital Diaphragm System (Photonic Instruments) was used to direct a 405 nm diode laser at the specimen plane. Typically, 1000 ms pulses were used with the laser at 100% for photobleaching of GFP and at 35% for photoconversion of tdEOS. Single focal planes were acquired at 3 or 5 s intervals for photobleaching and photoconversion experiments, respectively. Administration of taxol to cells being visualized was accomplished by the addition of 1 ml of CO_2-independent media containing 20 μM taxol to cells bathed in 1 ml of drug-free medium, yielding a final taxol concentration of 10 μM. Z stacks containing 5 focal planes with 2 μm spacing were acquired at 30 s intervals.

Analysis of FRAP Data

Time lapse FRAP sequences were first corrected for X-Y translation, using the StackReg ImageJ plugin. NIS-Elements (Nikon) was used to measure integrated fluorescence intensities of kinetochore-MT plus-end-bound Kif18A. Briefly, a 9×9 pixel square was placed over the region occupied by Kif18A, and the integrated fluorescence intensities for each frame were recorded in Excel (Microsoft). Background cytoplasmic fluorescence (F_{BG}) was determined by placing a second 9×9 pixel square near the kinetochore being analyzed. Background-corrected fluorescence intensity measurements were calculated by subtracting F_{BG} from Kif18A fluorescence at K-MT plus ends. Graphs of fluorescence intensities versus time were generated in SigmaPlot (Systat Software), and the resulting data fit to a single exponential, $F_t = F_0 + F_{inf} \times (1 - e^{-kt})$, essentially as described (Howell et al., 2000). F_0 represents the integrated fluorescence intensity of the photobleached region immediately after irradiation, and F_{inf} is the fluorescence intensity after maximal recovery. The half-life of fluorescence recovery was derived using the equation $t_{1/2} = \ln 2/k$. Mobile and immobile fractions of Kif18A at kinetochore-MT plus ends were calculated using the following equations:

$$F_m = (F_{inf} - F_0)/(F_I - F_0)$$

$$F_i = 1 - F_m$$

where F_m and F_i correspond to mobile and immobile fractions, respectively, and F_I is the integrated prebleach fluorescence intensity of Kif18A.

MT Gliding Assays and Kif18A-C307-MT Interaction Assays

Motility assays were performed and analyzed as described previously (Du et al., 2010). To visualize the interaction of Kif18A-C307-GFP with MTs in vitro, 400 ng protein was incubated with GMPCPP MTs (500 nM tubulin) in BRB80, 50 mM KCl, and 1 mM DTT for 30 min at room temperature (RT). Reactions were monitored by squashing 1 μl underneath an 18 × 18 mm coverslip and observing by fluorescence microscopy through a 100× 1.4 NA objective (Nikon).

For MT copelleting, 250 nM Kif18A-C307 was incubated with varying concentrations of taxol-stabilized GTP MTs in a 100 μl reaction consisting of 10 mM K-HEPES (pH = 7.7, 75, and 150) or 300 mM KCl, 1 mM DTT, and 1 μM taxol, for 15 min. The reactions were overlaid onto a 40% sucrose cushion prepared in assay buffer and spun at 60000 rpm for 20 min at 25°C in a TLA-100 rotor (Beckman). The supernatant was mixed with 100 μl 2× Laemmli buffer, and the pellet was solubilized in 200 μl 1× Laemmli buffer. Equal amounts of supernatant and pellet fractions were subjected to immunoblot analysis using anti-Kif18A and anti-α-tubulin followed by fluorescent anti-rabbit and anti-mouse secondary antibodies, respectively. Bound antibodies were detected and quantified using an Odyssey fluorescence detection system and analysis software (Li-Cor). Data were graphed in SigmaPlot and fit to a ligand-binding function, $y = (B_{max} \times x)/K_d + x$, to calculate the K_d of Kif18A-C307 for MTs.

TIRF Microscopy Assays

Analysis of single Kif18A molecules was performed using a Nikon TE2000-S inverted microscope, a 100× 1.49 NA Nikon TIRF objective, an Andor iXon DV 887 ECS-BV EMCCD camera, and a custom three-color TIRF illumination system. Single molecule experiments were performed in flow cells with taxol-stabilized MTs, grown from purified bovine brain tubulin labeled with Alexa 568 or Alexa 647, linked to PEG-silanized coverslips as previously described (Gestaut et al., 2008). TIRF experiments were carried out in BRB80 containing 1 mg/ml BSA, 10 μm taxol, an oxygen scavenging system (12 mM glucose + 2.5 mM DTT + 0.2 mg/ml glucose oxidase + 0.035 mg/ml catalase) and additional KCl. To analyze bleaching of GFP-tagged Kif18A motors, 20 pM Kif18A protein was added to MTs in the absence of nucleotide and imaged at 10 frames/s. For measurements of motility, 2 mM ATP, 50 pM GFP-Kif18A protein, and 75, 100, 125, 150, 200, or 250 mM KCl was added to the assay buffer, and frames were collected at 1–2 frames/s to prevent bleaching during long processive runs. For analyses of tail diffusion, 2 nM Kif18A-C307-GFP and 50 mM KCl were added to the assay buffer, and images were collected at 10 frames/s. Positional tracking and brightness measurements were carried out using custom programs written in LabVIEW, as previously described (Gestaut et al., 2008). Velocities were calculated via regression analyses of position versus time plots and obvious pause events were excluded.

To observe the effects of Kif18A proteins on the behavior of dynamic MTs, we used baculovirus-expressed rigor-kinesin (human Kif5B clone, residues 1–560 with G234A mutation, a gift of Frank McNally) to adhere MT seeds to PEG-silanized coverslips. Rigor-kinesin (0.1–0.4 mg/ml) diluted in BRB80 + 0.4–1 mg/ml casein was added to dry chambers and incubated for 5 min at RT. Chambers were then washed twice with BRB80 + 1 mg/ml casein and placed at 37°C. Unlabeled tubulin was polymerized at 7 mg/ml in BRB80 + 2 mM GTP + 5% DMSO, 30′ at 37°C, then diluted to 0.8 mg/ml tubulin in BRB80 + 1 mg/ml casein + 1.3 mM GTP and held at 37°C up to 3 hr. MTs were sheared by triturating twice through a 26s Hamilton syringe needle immediately before loading an observation chamber with 1 volume of MT solution for 5 min at RT. Unpolymerized tubulin at 0.8 mg/ml containing 0.5% Alexa 568-labeled tubulin was added to the chamber in GTP/ATP antifade buffer (BRB80 + 1 mg/ml casein + 1 mM ATP + 1 mM GTP + 12 mM glucose + 2.5 mM DTT + 0.2 mg/ml glucose oxidase + 0.035 mg/ml catalase) + 1/5× R buffer (R buffer = 300 mM KCl + 10 mM HEPES-KOH [ph 7.7] + 5% sucrose + 50 mM Arginine + 1 mM DTT + 0.1 mM ATP) + 0.1% methyl cellulose. Growth of labeled MTs was observed for 10 to 20 min, then GFP-Kif18A in a similar Alexa 568-tubulin/buffer/methyl cellulose solution was added, with GFP-Kif18A prediluted as needed in R buffer. Flow cells were observed using a Personal Deltavision microscope (Applied Precision) outfitted with 4-laser line TIRF capabilities, a 60× 1.49 NA TIRF objective (Olympus), and Ultimate Focus (Applied Precision) at 37°C. Images were collected at 2 s intervals using the 488 and 561 laser lines, sequentially, for 300 s total. The plus ends of individual MTs were tracked by hand using the softWoRx Explorer 1.3.0 (Applied Precision) two-point measuring tool. The time spent in assembly, disassembly, or pause was calculated for each MT as a ratio to the total observation time of 300 s or to complete MT disassembly, whichever came first. The data were graphed using Prism 5.0 (GraphPad Software, Inc.). Kymographs were prepared from representative MTs in ImageJ 1.42q (National Institutes of Health).

SUPPLEMENTAL INFORMATION

Supplemental Information includes six figures, one table, Supplemental Experimental Procedures, Supplemental References, and five movies and can be found with this article online at doi:10.1016/j.molcel.2011.07.022.

ACKNOWLEDGMENTS

We are grateful to Paul Miller, Gus Wright, and Emma Sturgill for technical advice regarding photomarking and to Ryan Lemke and Jeremy Cooper for technical assistance with single-molecule assays. We also thank Andy Powers, Kathy Gould, Sophia Gayek, and other members of the Dave Warshaw, Melanie Ohi, and Ryoma Ohi labs for critical review of the manuscript and insightful discussions, particularly during O'GOSH. tdEOS-C1 and tdEOS-N1 were kind gifts of I. Kaverina. This work was supported by funds from the Department of Cell and Developmental Biology at Vanderbilt University to R.O.; American Cancer Society IRG-58-009-50 to R.O.; NIH grants R01GM086610 to R.O., R01GM69429 to L.W., and R01GM79373 to C.A.; NSF grant 1041173 to L.W.; and a Ruth L. Kirschstein NRSA (GM778572) to J.S. J.S. is a Special Fellow of the Leukemia and Lymphoma Society. Implementation of 37°C TIRF capabilities on the Personal DV microscope was provided by Applied Precision, Issaquah, WA. The Quorum WaveFX spinning disk confocal system used in this study was acquired using funds provided by NIH grant S10RR025524.

Received: April 19, 2011
Revised: June 23, 2011
Accepted: July 28, 2011
Published: September 1, 2011

REFERENCES

Bormuth, V., Varga, V., Howard, J., and Schäffer, E. (2009). Protein friction limits diffusive and directed movements of kinesin motors on microtubules. Science *325*, 870–873.

Coy, D.L., Hancock, W.O., Wagenbach, M., and Howard, J. (1999). Kinesin's tail domain is an inhibitory regulator of the motor domain. Nat. Cell Biol. *1*, 288–292.

Du, Y., English, C.A., and Ohi, R. (2010). The kinesin-8 Kif18A dampens microtubule plus-end dynamics. Curr. Biol. *20*, 374–380.

Gestaut, D.R., Graczyk, B., Cooper, J., Widlund, P.O., Zelter, A., Wordeman, L., Asbury, C.L., and Davis, T.N. (2008). Phosphoregulation and depolymerization-driven movement of the Dam1 complex do not require ring formation. Nat. Cell Biol. *10*, 407–414.

Howell, B.J., Hoffman, D.B., Fang, G., Murray, A.W., and Salmon, E.D. (2000). Visualization of Mad2 dynamics at kinetochores, along spindle fibers, and at spindle poles in living cells. J. Cell Biol. *150*, 1233–1250.

Jaqaman, K., King, E.M., Amaro, A.C., Winter, J.R., Dorn, J.F., Elliott, H.L., McHedlishvili, N., McClelland, S.E., Porter, I.M., Posch, M., et al. (2010). Kinetochore alignment within the metaphase plate is regulated by centromere stiffness and microtubule depolymerases. J. Cell Biol. *188*, 665–679.

Mayr, M.I., Hümmer, S., Bormann, J., Grüner, T., Adio, S., Woehlke, G., and Mayer, T.U. (2007). The human kinesin Kif18A is a motile microtubule depolymerase essential for chromosome congression. Curr. Biol. *17*, 488–498.

Peters, C., Brejc, K., Belmont, L., Bodey, A.J., Lee, Y., Yu, M., Guo, J., Sakowicz, R., Hartman, J., and Moores, C.A. (2010). Insight into the molecular mechanism of the multitasking kinesin-8 motor. EMBO J. *29*, 3437–3447.

Poser, I., Sarov, M., Hutchins, J.R., Hériché, J.K., Toyoda, Y., Pozniakovsky, A., Weigl, D., Nitzsche, A., Hegemann, B., Bird, A.W., et al. (2008). BAC TransgeneOmics: a high-throughput method for exploration of protein function in mammals. Nat. Methods *5*, 409–415.

Savoian, M.S., and Glover, D.M. (2010). Drosophila Klp67A binds prophase kinetochores to subsequently regulate congression and spindle length. J. Cell Sci. *123*, 767–776.

Skibbens, R.V., Skeen, V.P., and Salmon, E.D. (1993). Directional instability of kinetochore motility during chromosome congression and segregation in mitotic newt lung cells: a push-pull mechanism. J. Cell Biol. *122*, 859–875.

Stumpff, J., von Dassow, G., Wagenbach, M., Asbury, C., and Wordeman, L. (2008). The kinesin-8 motor Kif18A suppresses kinetochore movements to control mitotic chromosome alignment. Dev. Cell *14*, 252–262.

Tischer, C., Brunner, D., and Dogterom, M. (2009). Force- and kinesin-8-dependent effects in the spatial regulation of fission yeast microtubule dynamics. Mol. Syst. Biol. *5*, 250.

Vale, R.D., Funatsu, T., Pierce, D.W., Romberg, L., Harada, Y., and Yanagida, T. (1996). Direct observation of single kinesin molecules moving along microtubules. Nature *380*, 451–453.

Varga, V., Helenius, J., Tanaka, K., Hyman, A.A., Tanaka, T.U., and Howard, J. (2006). Yeast kinesin-8 depolymerizes microtubules in a length-dependent manner. Nat. Cell Biol. *8*, 957–962.

Varga, V., Leduc, C., Bormuth, V., Diez, S., and Howard, J. (2009). Kinesin-8 motors act cooperatively to mediate length-dependent microtubule depolymerization. Cell *138*, 1174–1183.

Weinger, J.S., Qiu, M., Yang, G., and Kapoor, T.M. (2011). A nonmotor microtubule binding site in kinesin-5 is required for filament crosslinking and sliding. Curr. Biol. *21*, 154–160.

Molecular Cell, Volume *43*

Supplemental Information

A Tethering Mechanism Controls the Processivity and Kinetochore-Microtubule Plus-End Enrichment of the Kinesin-8 Kif18A

Jason Stumpff, Yaqing Du, Chauca A. English, Zoltan Maliga, Michael Wagenbach, Charles L. Asbury, Linda Wordeman, and Ryoma Ohi

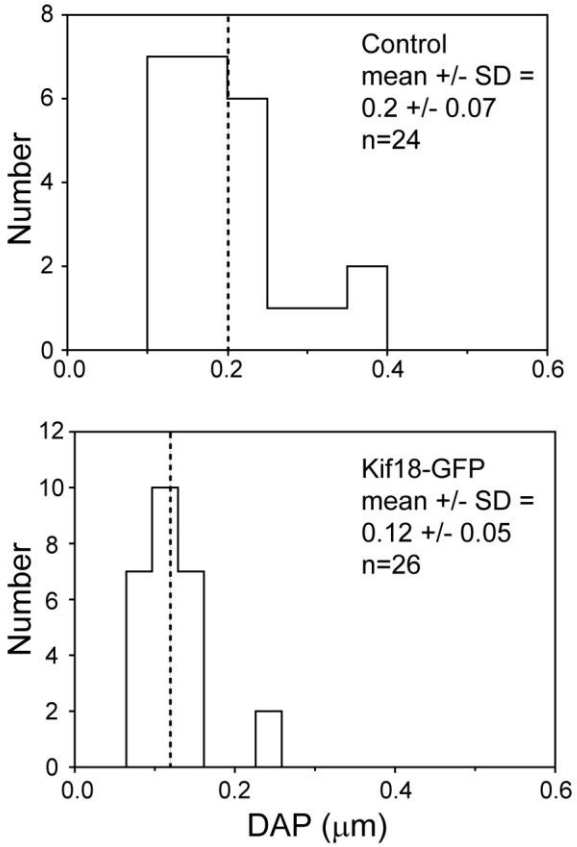

Figure S1, Related to Figure 1. Kinetochore Oscillation Dynamics in Kif18A-GFP Cells

Histograms showing deviation from average position (DAP) calculations for the indicated cell types. The mean ± SD is shown for each data set and the mean is marked by a vertical stippled line. n, number of kinetochores analyzed. The DAP for kinetochores in Kif18A-GFP cells are significantly different from the DAP for kinetochores in control cells ($p=1.37X10^{-5}$, two-sample t-test).

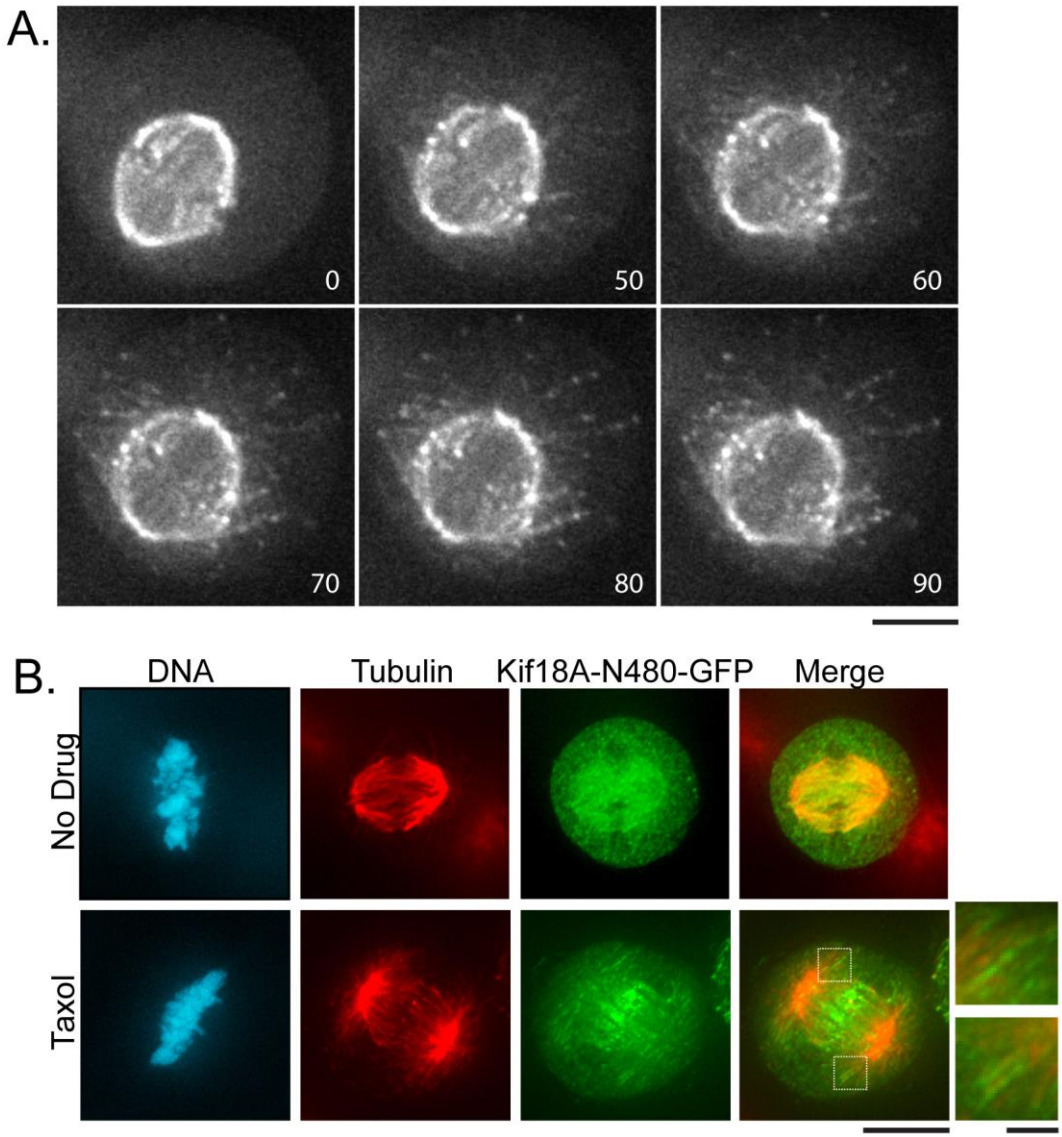

Figure S2, Related to Figures 1 and 2. Response of Kif18-GFP Proteins to Taxol Treatment

(A) Dynamics of Kif18A-GFP in a mitotic cell treated with 10 μM taxol. Time is indicated in seconds and is relative to taxol addition. Scale bar, 10 μm.

(B) The localizations of Kif18A-N480-GFP (green) and tubulin (red) in a mitotic HeLa cell treated with 10 μM taxol for 15 min are shown. Scale bars, 10 μm and 2 μm (enlarged images).

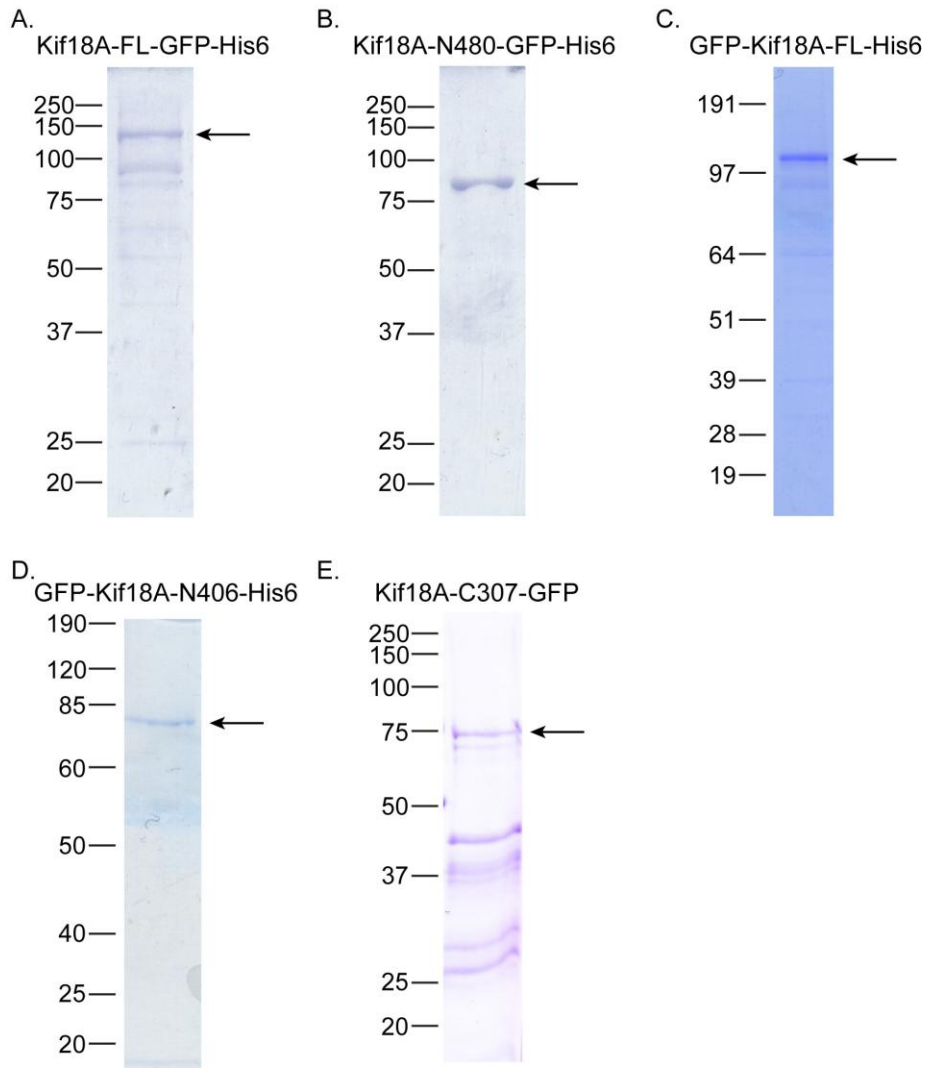

Figure S3, Related to Figures 3–6. Purification of Kif18A Proteins

Coomassie stained gels showing peak fractions from purifications of A) Kif18A-FL-GFP-His6 (MW = 129 kD), B) Kif18A-N480-GFP-His6 (MW = 82 kD), and C) GFP-Kif18A-FL-His6 (MW = 131 kD) from insect cells, as well as, D) GFP-Kif18A-N406-His6 (MW = 76 kD) and E) Kif18A-C307-GFP (MW = 61 kD) from bacteria. Expected products, which were confirmed by Western blots, are indicated by arrows and the positions of molecular weight markers (in kD) are indicated to the left of each gel.

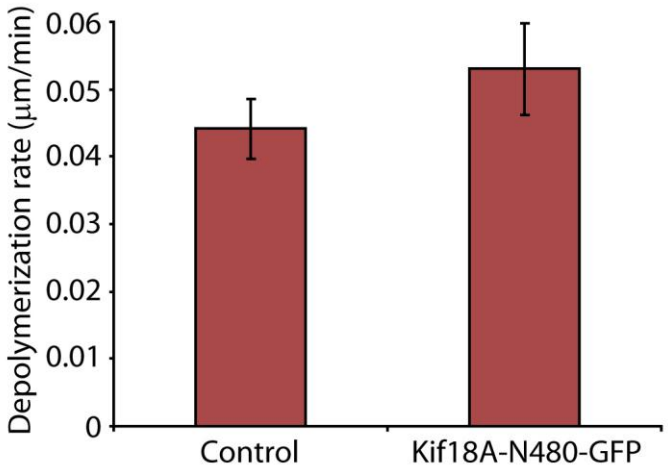

Figure S4, Related to Figures 3 and 6. Kif18A-N480-GFP Does Not Depolymerize GMPCPP MTs

Shortening rates of GMPCPP MTs treated with buffer or 250 nM Kif18A-N480-GFP are shown. Values are mean ± SEM.

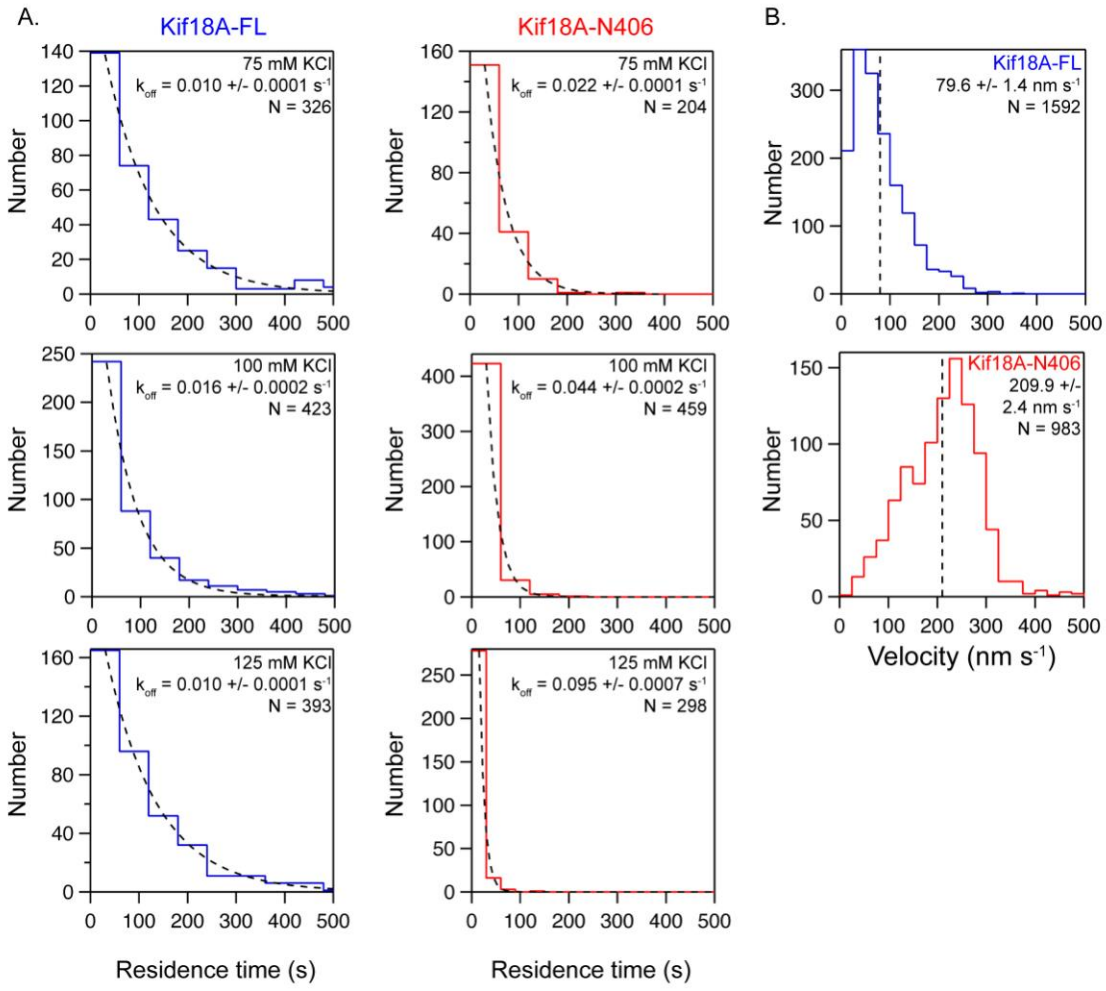

Figure S5, Related to Figure 3. The Dissociation Rate but Not the Velocity of GFP-Kif18A-N406 Is Sensitive to Ionic Strength

(A) Residence time distributions for GFP-Kif18A-FL and GFP-Kif18A-N406 single molecules on taxol MTs. Dissociation rates were calculated from exponential fits (dotted curves) to the distributions.

(B) Velocity distributions for the indicated motors measured in single molecule experiments. Distributions include measurements made under all salt concentrations tested since velocity did not vary significantly as a function of ionic strength (see Figure

3). The vertical dotted line indicates the mean ± SEM for each distribution. N = number of individual Kif18A particles analyzed.

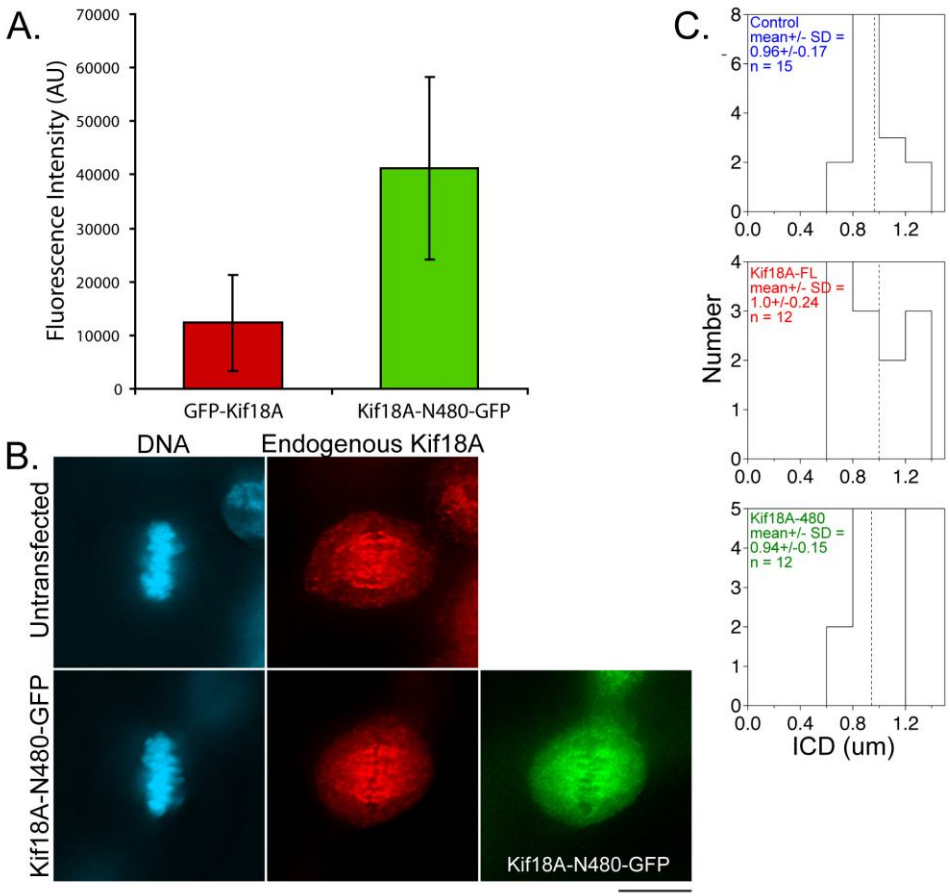

Figure S6, Related to Figure 7. Characterization of Cells Overexpressing GFP-Kif18A-FL and Kif18A-N480-GFP

(A) Mean fluorescence intensities (in arbitrary units) ± SD are shown. Data represent values obtained from four cells of each of the indicated cell types.

(B) Localizations of endogenous Kif18A (red) in a control or Kif18A-N480-GFP (green) expressing metaphase cell. Single deconvolved optical sections are shown. Scale bar, 10 µm.

(C) Histograms showing average intercentromere distances (ICD) for sister kinetochore pairs in the indicated cell types. The mean ± SD is shown for each data set and the mean value is marked by a vertical stippled line. n, number of kinetochores analyzed.

Table S1. FRAP analysis of Kif18A-GFP at KMT plus ends

Dynamic Parameters	
$t_{1/2}$	9.54±1.24 sec
Percent mobile fraction	70.43±3.11%
Percent stable fraction	29.57±3.11%

Kinetics of FRAP were analyzed as described in Materials and Methods. n=17 kinetochores. Values are mean ± SEM

SUPPLEMENTAL EXPERIMENTAL PROCEDURES

Molecular Biology and Baculovirus Construction

Plasmids mRFP-CENP-B, EGFP-C1-Kif18A, EGFP-N1-Kif18A-N480, and EGFP-C1-Kif18A-C307 have been described previously (Du et al., 2010; Stumpff et al., 2008). EGFP-N1-Kif18A was generated by PCR amplification of the complete Kif18A coding region and subcloning into the *Xho*I and *Bam*HI sites of pEGFP-N1 (Clontech). A second GFP-tagged tailless variant of human Kif18A, EGFP-C1-Kif18A-N406, was constructed by PCR amplification of codons 1-406 and subcloning using the Gateway cloning system (Invitrogen) into a modified version of pEGFP-C1 in which a Gateway RfA cassette (Invitrogen) was inserted into the Xho1 site of EGFP-C1 (Clontech). To construct EGFP-N1-Kif18A-C307, codons 591-898 were PCR-amplified and subcloned into the *Bgl*II and *Eco*RI sites of pEGFP-N1. Photoswitchable versions of full-length and N480 Kif18A were constructed by transferring the *Bam*HI/*Eco*RI Kif18A coding fragments from EGFP-C1-Kif18A and EGFP-N1-Kif18A-N480 into tdEOS-C1 and tdEOS-N1 (Wiedenmann et al., 2004), respectively.

pGEX6P-1-Kif18A-C307, which expresses the Kif18A tail fused to GST, was constructed by PCR amplification of codons 591-898 and subcloning into the *Eco*RI and *Bam*HI sites of pGEX6P-1 (Amersham). To create pGEX6P-1-Kif18A-C307-GFP, EGFP-N1-Kif18A-C307 was restricted with *Not*I, blunt-ended, and re-cut with *Bgl*II. The resulting fragment was subcloned into the *Bam*HI and *Sma*I sites of pGEX6P-1.

To construct pFastBac1-Kif18A-GFP-His_6, the Kif18A-GFP coding region was PCR amplified from EGFP-N1-Kif18A with a 3' oligonucleotide that inserts 6 histidine codons

in between the last GFP residue and the termination codon. This fragment was subcloned into the *Xho*I and *Bam*HI sites of pFastBac1 (Invitrogen). pFastBac1-Kif18A-N480-GFP-His_6 was prepared similarly except that the template for PCR was EGFP-N1-Kif18A-N480. pFastBac1-GFP-Kif18A-His_6 and pFastBac1-GFP-Kif18A-N406-His_6 were cloned by recombining GFP-Kif18A-FL-HIS6 and GFP-Kif18A-N406-HIS6 into the pDest8 plasmid using the Gateway cloning system (Invitrogen). pFastBac plasmids were used with the Bac-to-Bac system (Invitrogen) to create baculoviruses that express Kif18A-FL-GFP-His_6, Kif18A-N480-GFP-His_6, GFP-Kif18A-FL-His_6, and GFP-Kif18A-N406-His_6. For expression of GFP-Kif18A-N406-HIS_6 in bacteria, a pET-GFP-Kif18A-N406-HIS_6 was constructed by recombining the Kif18A-N406-HIS_6 sequence into a modified pET30 vector containing an EGFP sequence inserted in the *Xho*1 site and a Gateway Rfb cassette cloned into the *Hind*III site.

Protein Expression and Purification

GST-Kif18A-C307 and GST-Kif18A-C307-GFP were expressed in BL21-CodonPlus(DE3)-RIPL cells (Stratagene). For purification, cells were resuspended in lysis buffer (PBS, 300 mM NaCl, 1% IGEPAL CA-630, 5 mM β-mercaptoethanol, and protease inhibitors [1 mM phenylmethylsulfonyl fluoride; 1 mM benzamidine; and 10 μg/ml each of leupeptin, pepstatin, and chymostatin]) containing 1 mg/ml lysozyme. Lysate was sonicated and clarified by centrifugation at 35,000 rpm for 1 hour in a Ti 50.2 rotor (Beckman). ~2 ml of glutathione agarose was incubated with the supernatant for 1 hour at 4°C, and then washed extensively with lysis buffer lacking IGEPAL CA-630 and protease inhibitors. The resin was then washed into cleavage buffer (10 mM Tris-

Cl, pH=7.0, 150 mM NaCl, 1 mM EDTA, 1 mM DTT) and treated overnight at 4°C with PreScission protease (GE Healthcare). Eluted protein was dialyzed into 10 mM K-HEPES, pH=7.7, 300 mM KCl, 1 mM DTT, aliquoted, frozen in liquid N_2, and stored at -80°C.

GFP-Kif18A-N406-HIS_6 was expressed in BL21 cells. Cells were then frozen in liquid nitrogen and ground to a powder with a mortar and pestle. Frozen cell powder was resuspended in lysis buffer (20 mM imidazole pH 7.0, 300 mM KCl, 1 mM $MgCl_2$, 0.1 mM ATP, 10% glycerol, 1 mM PMSF and EDTA-free protease inhibitor cocktail (Roche)). Lysates were run through a french press and then cleared by spinning at 10,000 RPM in a JA-14 rotor for 10 minutes followed by 35,000 RPM in a Ti45 for 60 minutes. Supernatants were incubated with 5 ml of Ni-NTA resin for 1 hour at 4ºC and then washed extensively in a glass column with pH 8.0 wash buffer (20 mM imidazole pH 8.0, 0.01 mM ATP and 300 mM KCl). Proteins were eluted by addition of elution buffer (250 mM imidazole, 300 mM KCl, 0.2 mM $MgCl_2$, 0.01 mM ATP and 10% glycerol) and collected in 4 ml fractions. Peak fractions were pooled and dialyzed into storage buffer (20 mM PIPES pH 6.8, 300 mM KCl, 1 mM $MgCl_2$, 1 mM EGTA, 0.01 mM ATP and 10% glycerol) and snap frozen in working aliquots.

Full-length Kif18A-His_6 was expressed in *Sf*-9 cells and purified as described previously (Du et al., 2010) except that all solutions excluding the lysis buffer were supplemented with 50 mM arginine and 50 mM glutamate. Kif18A-GFP-His_6 GFP-Kif18A-FL-HIS_6, GFP-Kif18A-N406-HIS_6 and Kif18A-N480-GFP-His_6 were expressed for 72 h in *Sf*-9

cells. Kif18A-GFP-His_6, GFP-Kif18A-FL-His_6 and GFP-Kif18A-N406-His_6 were purified as Kif18A-His_6 except that the motors were not subjected to size exclusion chromatography. Following elution from Ni_2+-NTA agarose (Qiagen), the motor was immediately buffer-exchanged into 10 mM K-HEPES, pH=7.7, 300 mM KCl, 1 mM DTT, 0.1 mM MgATP using a PD-10 column (GE Healthcare). Kif18A-N480-GFP-His6 was also purified similarly to Kif18A-His_6 but all buffers for purification contained 50 mM arginine. The Ni2+-NTA eluate was immediately buffer-exchanged into 10 mM K-HEPES, pH=7.7, 300 mM KCl, 50 mM arginine, 1 mM DTT, 0.1 mM MgATP using a PD-10 column, and subjected to size exclusion chromatography on a Superose 12 column (GE Healthcare) equilibrated in same buffer. All motor concentrations were determined using Bradford assays and take into account that Kif18A exists as a dimer in solution (Du et al., 2010). Powdered sucrose (20%) was added, and the protein aliquoted, frozen in liquid nitrogen, and stored at -80°C.

Axoneme Regrowth Assay

Tetrahymena axonemes (Mitchison and Kirschner, 1984) were used to nucleate MTs in a reaction mixture containing BRB80, 75 mM KCl, 1 mM DTT, 20 μM tubulin, 1 mM GTP, and 1 mM MgATP. When necessary, Kif18A-GFP or Kif18A-N480-GFP were added to reactions to a final concentration of 500 nM. MT polymerization was induced by incubating the reactions at 37°C for 20 min. Regrown axonemes were fixed with 3 volumes of 1% glutaraldehyde prepared in BRB80 at 37°C for 3 minutes, and then diluted into 1 ml of BRB80. Reactions were overlaid onto 10% glycerol cushions in 15 ml Corex tubes containing a chock and a 12 mm poly-L-lysine coated coverslip, and

spun onto poly-L-lysine-coated coverslips at 10,000 rpm for 20 min in a JS 13.1 rotor (Beckman). Coverslips were post-fixed in methanol at -20°C for 1 minute, rehydrated in TBS containing 0.1% Triton X-100 (TBST) and treated with sodium borohydride to quench free aldehydes. Coverslips were then incubated with mouse anti-α-tubulin (1:500; Sigma) followed by Alexa 594-labeled secondary antibodies. Axonemal MTs were photographed with an NIS Elements controlled Eclipse 90i (Nikon) equipped with a 100X 1.4 NA objective (Nikon) and a CCD camera (Roper). MT lengths were determined using NIS Elements image analysis software and for each case, data was collected from 2-3 independent experiments.

Immunofluorescence and Deconvolution

HeLa cells were fixed with methanol at -20°C for 10 minutes. To preserve GFP fluorescence, 1% paraformaldehyde was added to ice-cold methanol for some experiments. Cells were labeled with the following primary antibodies: rabbit anti-Kif18A (1 µg/ml; (Du et al., 2010)), mouse anti-α-tubulin (1:500; Sigma), rat YL1/2 (1:500; Accurate Chemical) human CREST serum (1:1000; Immunovision), or Alexa 488-conjugated anti-GFP (1:1000; Rockland) for 1 h at room temperature. Anti-mouse, anti-rabbit, anti-rat, and anti-human secondary antibodies conjugated to Alexa 488 or Alexa 594 (Invitrogen) were used at 1:1000 for 45 min. To localize Kif18A in fixed taxol-treated cells, HeLa cells were treated with 10 µM taxol for 15 minutes prior to methanol fixation. DNA was counterstained with 5 µg/ml Hoechst 33342. Stained cells were mounted in Prolong (Invitrogen) or Vectashield (Vector) and imaged using a Deltavision Core system equipped with a CCD camera and 60X 1.4 NA or 100X 1.4 NA objectives

(Olympus). Z-stacks were taken with 0.2 or 0.3 µm spacing and deconvolved using a Deltavision workstation.

SUPPLEMENTAL REFERENCES

Du, Y., English, C.A., and Ohi, R. (2010). The kinesin-8 Kif18A dampens microtubule plus-end dynamics. Curr Biol *20*, 374-380.

Mitchison, T., and Kirschner, M. (1984). Dynamic instability of microtubule growth. Nature *312*, 237-242.

Stumpff, J., von Dassow, G., Wagenbach, M., Asbury, C., and Wordeman, L. (2008). The kinesin-8 motor Kif18A suppresses kinetochore movements to control mitotic chromosome alignment. Dev Cell *14*, 252-262.

Wiedenmann, J., Ivanchenko, S., Oswald, F., Schmitt, F., Rocker, C., Salih, A., Spindler, K.D., and Nienhaus, G.U. (2004). EosFP, a fluorescent marker protein with UV-inducible green-to-red fluorescence conversion. Proc Natl Acad Sci U S A *101*, 15905-15910.